Role of Cationic Organisation on Water Dynamics in Saponite Clays

V. Marry,[*,†] S. Le Crom,[†] E. Ferrage,[‡] L. Michot,[†] B. Farago,[¶] A. Delville,[§] and E. Dubois[†]

†*Sorbonne University, Laboratoire PHENIX UMR CNRS 8234, 4 place Jussieu, case 51, 75005 Paris, France*

‡*IC2MP-Hydrasa, UMR 7285, CNRS, Université de Poitiers, 5 rue Albert Turpain, Bât. B8, TSA 51106, 86073 Poitiers cedex 9, France*

¶*Institut Max von Laue-Paul Langevin (ILL), 71 Avenue des Martyrs, CS 20156, F-38042 Grenoble Cedex 9, France*

§*ICMN, UMR 7374, CNRS-Universite d'Orléans, 1b rue de la Férollerie, CS 40059, 45071 Orléans cedex, France*

E-mail: virginie.marry@sorbonne-universite.fr

Abstract

Water dynamics impacts many phenomena from geosciences to biology, especiallly in confined environments. In the presence of charged interfaces, there are some ions the role of which with regards to the water dynamics is unclear. Here a synthetic saponite clay, which is oriented in a film, is used as confining medium in the bilayer state. It confines two water layers between negatively charged planes, the charge of which is compensated by sodium cations. Water dynamics is determined both parallel and perpendicular to the charged clay layers with Neutron Spin Echo (NSE). This technique gives access to long enough times and directly provides the intermediate

scattering function that is calculated on the other hand by Molecular Dynamics (MD) simulations. These latter also enable the study of cations dynamics, not experimentally accessible on this time scale. The results point towards a huge role of these cations on the water dynamics, mainly through their local structure and localization between the charged confining planes.

Introduction

A vast body of literature focuses on the properties of water in a confined environment, a situation highly different from that of bulk water.[1–8] Changes associated to confinement are of prime importance in numerous fields such as, among others, separation, energy storage, catalysis, protein dynamics, biomolecules, or nanofluidic. Numerous matrices are thus relevant from 0D ones such as reversed micelles or fullerene,[4,6,8–10] 1D such as nanotubes[4,8,9,11,12] or 2D like graphene, MoS_2 or clay minerals.[6–8,13] In these confined matrices, the behaviour of the fluid depends on both surface properties and dimensionality,[4,6,7,9] that can be investigated separately, by coupling experiments and numerical simulations. The influence of dimensionality was for instance analyzed by molecular dynamics in 0D, 1D and 2D matrices[10] whereas the role of interfaces can be explored without confinement.[14]

Among the 2D matrices, swelling clay minerals are natural 2D systems that bear high industrial and environmental relevance. In these materials, two tetrahedral layers sandwich an octahedral one. Substitutions in either the octahedral or tetrahedral layer yield an overall negative charge that is compensated by hydrated exchangeable cations. The valence and hydration properties of these interlayer cations control to a large extent the swelling of the structure that occurs in a stepwise way with increasing relative humidity, a feature that has been known for almost a century.[15] This swelling regime referred to as crystalline swelling[16] provides an elegant way to control water confinement in the structure as, depending on humidity, confinement accounts for either one or two statistical layers of water molecules corresponding to the so-called monolayer and bilayer states. Numerous experimental and

simulation studies have investigated the structure and dynamics of water in this swelling regime.[17–21] Convincing results were obtained by focusing on synthetic clay minerals such as saponite and hectorite that are less heterogeneous than natural samples, a significant advantage on both experimental (less hydration heterogeneities) and simulation (more realistic models) points of view.[22–27] In all the studies dealing with the structure of confined water, it appeared crucial to collate experiments results with simulation ones to test extensively the suitability of the various force fields used in the simulations. Furthermore, as far as dynamics are considered, considering motion anisotropy by working on oriented samples proved particularly fruitful.

Regarding the experimental assessment of dynamics, neutron spin echo (NSE) bears definite advantages over the more commonly used time-of-flight (TOF) neutron scattering technique, especially for anisotropic oriented samples as those studied here. Indeed, NSE experiments directly yield the intermediate scattering function in a time range extending up to a few nanoseconds, i.e. a value higher than that accessible by TOF measurements, which facilitates the direct comparison with Molecular Dynamics (MD) simulations.

In the present paper, using a combination of NSE experiments and MD simulations with various force fields and water models, we analyze in detail for various temperatures the dynamical features of water molecules confined in the interlayer space of an oriented sodium saponite sample for a water content corresponding to a bilayer. Collating experimental results and MD simulations allows evaluating the orientational dynamical features. We show in particular that the location of cations in the interlayer space plays a significant role on the diffusion coefficients of water molecule. This could well explain why measured and simulated diffusion coefficients are different in tetrahedrally substituted clay samples compared to octahedrally substituted materials.

Experiments

Preparation of the oriented clay films

The sample used in the present study is a synthetic saponite sample prepared by hydrothermal treatment [28] with a general formula of $Si_{7.2}Al_{0.8}Mg_6O_{20}(OH)_4Na_{0.8}H_2O_n$. The orientation of the clay platelets was achieved by slow drying of clay suspensions on a surface larger than 4cm*3cm, which produces thin films (around 15 microns). The samples thus obtained were first equilibrated in a relative humidity RH ∼98% (using a $CuSO_4$ saturated solution vapor) and then equilibrated for two weeks at RH∼75% (NaCl solution) to obtain a bihydrated state while minimizing hydration heterogeneity, in agreement with our previous X-ray and neutron diffraction study on the same sample. [24] The oriented thin films were stacked until the total amount of water is equivalent to around 0.15 mm of pure water. According to our previous works on the same samples, [24,25,29] bihydrated saponite displays at this RH condition a d-spacing of ∼15.20 Å and n≃9.57 interlayer H_2O molecules. [25]

Neutron Spin Echo Measurements

Neutron spin echo (NSE) experiments were performed on the IN15 spectrometer (ILL, Grenoble, France). The wavelength is 6.3 Å and the accessible time scale expands from 8 ps to 10 ns. The wavevectors Q lie in the range 0.2 $Å^{-1}$ to 1.2 $Å^{-1}$. The temperature is controlled with a cryostat and 3 values were chosen: 300 K, then 255 K and/or 350 K.

The films were sealed in an aluminium cell with an indium seal. The number of thin films stacked was adapted to the hydration in order to obtain an equivalent water thickness around 0.15 mm. The thickness of the cell was chosen thick enough to avoid breaking the films. The cell was oriented either with Q parallel to the clay layers, or with Q perpendicular to the clay layers, for each measured Q value. In the latter case, only Qs between 0.6 and 1.2 $Å^{-1}$ are accessible for geometrical reasons. NSE experiments directly yield the intermediate scattering function in a time range extending up to a few nanoseconds, i.e. a value higher than

that accessible by Time of Flight measurements. This is well adapted for the slow motions as the one seen here and facilitates the direct comparison with Molecular Dynamics (MD) simulations. In addition, as the energy exchange is very small, the momentum exchange (scattering vector) also changes very little in magnitude as well as in orientation, which is an advantage for oriented samples.

The scattered intensity S(Q,0) as a function of Q was obtained in both the parallel and perpendicular directions (Figure 1). The Bragg peak corresponding to the interlayer spacing appears only when Q is perpendicular to the plane of the aluminum cell, which indicates a good orientation of the clay sheets. The peak position is consistent with the known values, determined from X-Rays diffraction at Q= 0.413 $Å^{-1}$ for the bilayer state which corresponds to 15.21 Å d-spacing, as expected for a bilayer state. The orientation of the clays is confirmed and quantified from a measurement of mosaicity (see Figure 2). The half width at half maximum (HWHM) of the peaks is 8.8° for this bilayer state. The degree of anisotropy in particles orientation can thus be extracted by calculating the average of the second-order Legendre polynomial of this distribution[30] as: $\langle P_2 \rangle = \langle P_2(\cos\theta) \rangle = \langle 3\cos^2\theta - 1 \rangle / 2$. The high value obtained for $\langle P_2 \rangle$ of 0.94 pleads for a high degree of preferred orientation of clay platelets.[30]

Sample integrity was periodically checked by carrying out scans at a zero spin echo time in the perpendicular direction. This allowed verifying the d-spacing of the studied sample and discarding possible leaks in the cell. No significant evolution of layer thickness was observed when changing the temperature, and their respective water content was thus constant for all temperatures investigated.

For $S(Q,t)$ measurements, the Q values are chosen in order to avoid the Bragg peak so that the incoherent scattering contribution dominates. In the parallel direction, Q=0.2, 0.3 and 0.6 $Å^{-1}$ are thus chosen (see Figure 1). The signal of an empty cell is measured and subtracted from the signal of the sample, and the resolution is measured on a graphite/TiZr

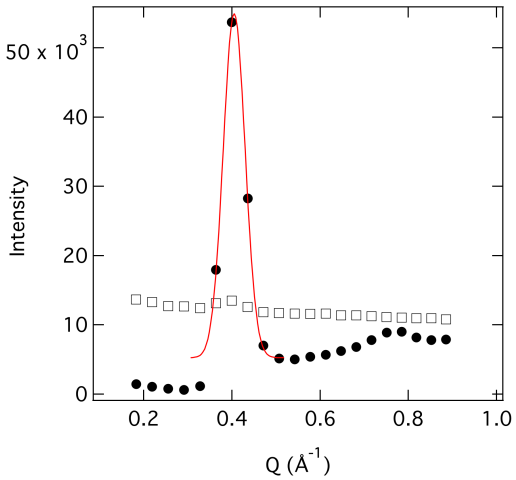

Figure 1: Intensity scattered at a spin echo time zero by the clay film as a function of Q for the bilayer state for the two orientations of the cell. Cell perpendicular to the scattering vector Q (circles) or parallel to Q (empty squares).

sample. At the end, the incoherent intermediate scattering function $S_{inc}(Q,t)$ is obtained. The data are plotted with markers on all the following figures whereas the calculated curves are plotted with lines.

Model for the analysis

In the most general case, assuming that short-time dynamics (vibrations, librations), rotation dynamics and translational diffusion are decoupled mechanisms, $S(Q,t)$ takes the form of:

$$S(Q,t) = S_{vib}S_{rot}S_{trans} \tag{1}$$

S_{vib} is the vibrational incoherent scattering function. It tends towards a plateau at very small times (inferior to about 2 ps) hardly accessible by NSE experiment and can be approximated by a multiplying factor independent of t, which decreases with Q.

S_{rot} is close to unity as soon as Q is not too big. The usually accepted limit to consider $S_{rot} = 1$ is $Q = 1$ Å^{-1} for water.[31,32] In the following, rotational motions will be neglected, even if this approximation could be questioned for the highest Q (1.2 Å^{-1} for Q_{perp}).

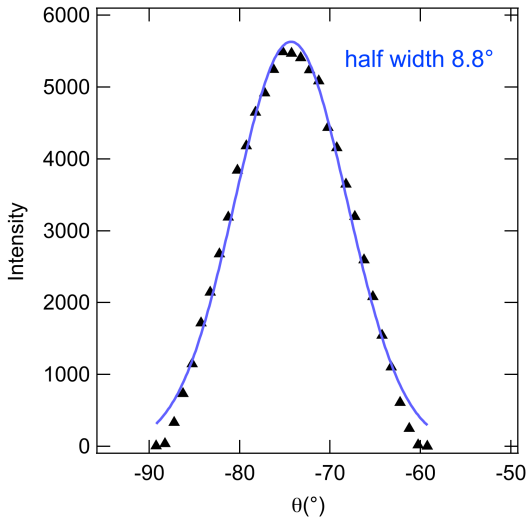

Figure 2: Mosaicity of the film in the bilayer state: scattering measured while rotating the sample around the position of the Bragg peak corresponding to the interlayer distance. Q=0.41Å^{-1} and the sample is oriented so that Q is perpendicular to the clay layers on the Bragg peak.

At last, in the case of pure diffusion, S_{trans} can be fitted by decreasing monoexponential:

$$S_{trans}(Q,t) = \exp^{-t/\tau} \tag{2}$$

with the relaxation time τ varying with Q as:

$$\frac{1}{\tau} = DQ^2 \tag{3}$$

D being the self-diffusion coefficient of hydrogen atoms. In reality, this last equation is valid only at small Qs. Experimentally, because water has complex diffusion mechanisms, especially in confined systems, $S_{trans}(Q,t)$ contains several relaxation times and is better fitted by a stretched exponential:

$$S_{trans}(Q,t) = \exp^{-(t/\tau)^{\beta}} \tag{4}$$

β tends towards 1 when Q goes to 0. Indeed, small Qs correspond to high observation distances at which water molecules diffuse with a diffusion coefficient that averages all the

different motion mechanisms.

Added to this are the (quasi-)immobile H atoms contained in the hydroxyl groups of the clay layers, that do not diffuse and are responsible for a plateau at high NSE times.

Considering short-time motions and immobile H atoms, $S(Q,t)$ can be reduced to:

$$S(Q,t) = (A-B)\exp^{-(t/\tau)^{\beta}} + B \tag{5}$$

A and B are the limits of $S(Q,t)$ at short and high times, respectively. The average relaxation time $\langle\tau\rangle$ can then be calculated from $\langle\tau\rangle = \frac{\tau}{\beta}\Gamma(\frac{\tau}{\beta})$, where Γ is the gamma function. In this case, the slope of $1/\langle\tau\rangle$ as a function of Q^2 decreases with Q and is usually fitted in the literature by a jump-diffusion model where $1/\langle\tau\rangle$ tends at high Qs towards a plateau equal to $1/\tau_{jump}$, corresponding to a non-diffusive process where the molecule stays immobile for a time τ_{jump} before jumping from one site to the other one. If a range of relaxation times partly explains the curvature of $\langle\tau\rangle$ as a function of Q^2, it has already been shown in the literature that the curvature depends strongly on the resolution of the apparatus[25,33,34] and that more complex models are needed to describe water diffusion mechanism, and even more in confined systems.[35,36] However, the average diffusion coefficient can be deduced from the slope of $1/\langle\tau\rangle$ at very small Qs.

Moreover, in the case of clays, water motions are not equivalent in all directions: because of the symmetry of the system, at least two motions, one parallel and one perpendicular to the clay layers, must be distinguished. Even in the case of oriented samples like in the present study, the orientations of the clay layers cannot be perfect and a mosaicity of the orientations must be taken into account. As a consequence, the value of β and $1/\langle\tau\rangle$ obtained with the above formula can be affected by mosaicity.

In our previous studies,[26,37] a two-diffusion model considering two diffusion coefficients $D_{\parallel}$ and $D_{\perp}$ for the motions parallel and perpendicular to the clay layers respectively, averaged over all the possible orientations of the clay layers, was used to fit the experiments. Even if the hypothesis of this rather crude model according to which the hydrogen density is

homogeneous in the pore is questionable due to the structuration of the fluid (see figure 10), it has shown that motions perpendicular to the clay layers absolutely had to be taken into account to analyze the experimental results in the case of powder samples. The molecular simulations allowed constraining the value of $D_{\parallel}/D_{\perp}$.

In the present study, this two-diffusion model is used in order to study the influence of mosaicity and to help the interpretation of the data too. θ being the angle between the normal to the clay layer and the Q vector, an average over all orientations can be done considering a Gaussian distribution of θ around θ_0, θ_0 corresponding to the main orientation of the clay layers. The probability to find a clay layer with an orientation θ can be defined as:

$$P(\theta) = P_0 \mathrm{e}^{-(\frac{(\theta-\theta_0)}{\Delta\theta})^2} \tag{6}$$

with $\Delta\theta$ accounting for the mosaicity. In the following, a value of 10° was taken for $\Delta\theta$, corresponding to a half width at half maximum (HWHM) of the probability $P(\theta)$ of 8°, very close to the experimental one (see Figure S1 in SI). P_0 is a factor such that the integral of $P(\theta)$ is equal to 1. The value of θ_0 is 0° and 90° for the analysis of $S(Q_{\perp}, t)$ and $S(Q_{\parallel}, t)$ respectively. The modelled $S^{mod}(Q,t)$ can be calculated numerically using (see SI for details):

$$\begin{aligned} S^{mod}(Q,t) = 2\mathrm{e}^{-D_{\parallel}Q^2 t} \Bigg[\int_0^{\pi} \mathrm{e}^{D_{\parallel}Q^2\cos^2\theta t} \frac{(1-\cos(QL\cos\theta))}{Q^2L^2\cos^2\theta} P(\theta)\mathrm{d}\theta \\ + \sum_{n=1}^{\infty} 2\mathrm{e}^{-\frac{n^2\pi^2 D_{\perp} t}{L^2}} \int_0^{\pi} \mathrm{e}^{D_{\parallel}Q^2\cos^2\theta t} \frac{[Q^2L^2\cos^2\theta(1-(-1)^n\cos(QL\cos\theta))]}{(n^2\pi^2 - Q^2L^2\cos^2\theta)^2} P(\theta)\mathrm{d}\theta \Bigg] \end{aligned} \tag{7}$$

Molecular dynamics simulations

The interactions between atoms were described using clayFF force field for the clay.[38] The atoms interact via a Coulombic potential and a Lennard Jones potential, according to:

$$V_{ij} = \frac{q_i q_j}{4\pi\epsilon_0 r_{ij}} + D_{0,ij}\left[\left(\frac{R_{0,ij}}{r_{ij}}\right)^{12} - 2\left(\frac{R_{0,ij}}{r_{ij}}\right)^{6}\right] \quad (8)$$

where q_i is the partial charge of atom i and $D_{0,ij}$ and $R_{0,ij}$ energy and distance parameters characteristic of couples (i,j). As for previous simulations on fluoro-hectorite systems,[23,26] the charge of the octahedral magnesium was kept to 1.36 and the charge of apical surrounding oxygen atoms was adjusted to -1.2825 in order to ensure the neutrality of the clay layers.[39]

The original water model used in clayFF is a flexible version of SPC.[38,40] Despite the fact that flexibility could play a role on energy exchanges between water and clay layers which could affect the dynamics, we chose in previous studies to use the rigid model of water TIP4P2005[41] because this water model yields accurate diffusion coefficients on a large range of temperatures.[23] In this case, the Lennard-Jones parameters for the interactions between the clay oxygens and the fluid species (water and sodium ions) were taken to be the same as between water and fluid species, without modifying the interactions internal to the clay layers.

In order to study the effect of the force-field on the properties of the interlayer fluid, we also performed simulations with the clayFF force-field modified by Ferrage et al.[24] and the flexible SPC water as in Michot et al[25] . The authors used it in order to analyze time-of-flight experiments on the same sample, in a very similar approach to ours, and showed very good quantitative agreement with measurements. In this force-field, the $R_{0,ij}$ between the fluid and the oxygen atoms of the clay surface were increased in order to fit better XRay and neutron diffraction experiments.[24]

The simulations were done with the LAMMPS simulation package.[42] The simulation box contained four clay layers of 84 elementary cells each. 272 Na^+ ions and 3217 water molecules were equally distributed in the four interlayer spaces, corresponding to a negative cell charge of -0.81 e and to a water content of 11.83 H_2O per cation. An example of snapshot is given in Figure S2 of SI. The vertical dimension of the box was fixed to 60.8 Å, which corresponds to the average interlayer spacing of 15.4 Å of the bilayer state. The water content and interlayer

spacing were chosen to be equal to the experimental values obtained by X-Ray diffraction on a saponite of same charge.[29] Periodic boundary conditions were used with electrostatic interactions computed using Ewald summation.

After a phase of equilibration of 500 ps, 20 ns simulations were performed at the three temperatures of interest, 255, 300 and 350 K in NVT ensemble. The timestep was 1 fs. The temperature was maintained with a Nose-Hoover type thermostat, with a time constant of 1 ps.

From the trajectories, diffusion coefficients parallel to the clay layers could be obtained from the slope of the horizontal mean-squared displacement (MSD) on a time interval between 300 ps and 9 ns where the MSD is linear, using:

$$D_{\parallel} = \lim_{t\to\infty} \frac{\langle x(t)^2 + y(t)^2 \rangle}{4t} \tag{9}$$

$x(t)$ and $y(t)$ refer to the displacements of a particle between 0 and t along x and y, and the brackets to averages over all the atoms of a same type and the origins of times.

Assuming homogeneous distribution of HW atoms in the pore, diffusion coefficients perpendicular to the clay layers could be estimated by calculating the slope with time of the $\Psi(t)$ autocorrelation function:[26,43]

$$\left(\frac{L}{\pi}\right)^2 \ln < \Psi(t)\Psi(0) >= -D_{\perp} t \tag{10}$$

with

$$\Psi(t) = \sqrt{2}\cos\left(\pi \frac{z(t) - z_{min}}{L}\right) \tag{11}$$

where $z(t)$ is the vertical position of the atom at time t and $L = z_{max} - z_{min}$, z_{max} and z_{min} are the positions of the walls, *i.e* the positions in the interlayer where the densities of the atoms cancel. Despite the hypothesis according to which the density is homogeneous in the pore, the autocorrelation function defined above have already shown good linear behavior

which suggests that the perpendicular diffusion coefficient thus calculated is a reasonable parameter to describe on average the motion perpendicular to the clay layers.[26]

Similarly, incoherent scattering functions $S(Q,t)$ could be calculated using the expression of the autocorrelation function:

$$S(Q,t) = \langle \mathrm{e}^{i\mathbf{Q}.\mathbf{r}(\mathbf{t})} \mathrm{e}^{-i\mathbf{Q}.\mathbf{r}(\mathbf{0})} \rangle \tag{12}$$

where $\mathbf{r}(\mathbf{t})$ is the position of the atom at time t. In this case, the brackets refer to averages over all the atoms of a same type and the origins of times, but also to averages over various orientations of the wavevector $\mathbf{Q}$. In order to compare with the experiments made with oriented samples, $\mathbf{Q}$ was chosen to be parallel (or perpendicular) to the clay layers. In order to take into account sample mosaicity, $S(Q,t)$ was averaged over more than one hundred random orientations of $\mathbf{Q}$ chosen in such a way that the angles between $\mathbf{Q}$ and XY plane (or Z axis) satisfy the Gaussian distribution $P(\theta)$ of equation 6. It was checked that increasing the number of orientations did not affect the $S(Q,t)$ curves.

Results

Diffusion parallel to the clay layers at T=300 K

Firstly, experimental $S_{\parallel}(Q,t)$ were fitted with equation 5. The fraction of immobile H atoms, corresponding to an hydration state of 11.83 H_2O per cation, is 0.17, in between the fitted values of B going from 0.11 to 0.22. However, the observed dispersion between the experimental plateau values at high times (figure 4) could not find a satisfactory explanation. The exponent β was found to be equal to 1 for $Q = 0.2$ and $Q = 0.3$ Å^{-1} and 0.95 for $Q = 0.6$ Å^{-1} (however β=1 also gives a very good fit). $1/\langle\tau\rangle$ as a function of Q^2 is plotted on figure 3.

As usually observed in this type of systems, the slope of $1/\langle\tau\rangle$ decreases with Q^2. Fitting

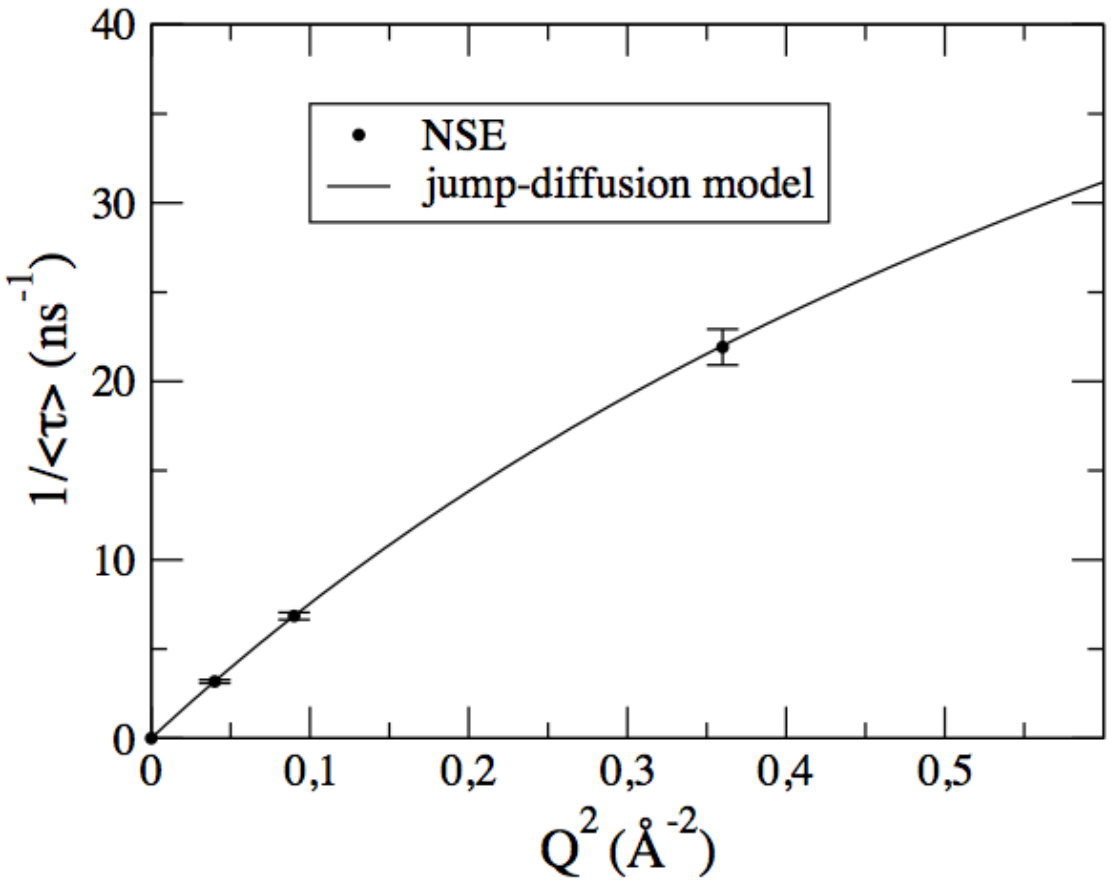

Figure 3: Inverse of averaged relaxation time as a function of Q^2 obtained by fitting experimental $S_{\parallel}(Q,t)$ with equation 5. Points: NSE experiment, solid line: jump-diffusion model.

experimental $1/\langle\tau\rangle$ by the widely used jump-diffusion model:

$$\frac{1}{\langle\tau\rangle} = \frac{DQ^2}{1 + DQ^2\tau_0} \tag{13}$$

leads to a value of D=8.3±0.3.10^{-10} m^2.s^{-1} and τ_0=12±3 ps. As mentioned in the previous section, this time strongly depends on the resolution of the apparatus[25,33,34] which makes it difficult to comment and compare with the literature. In the present study, the determined $\langle\tau\rangle$ is correct at low Q and could be overestimated at large $Q = 0.6$ Å^{-1} as the fastest water molecules are outside of the accessible times with IN15 on this lengthscale. This introduces an error on the determination of τ_0 but also on the diffuson coefficient D, both depending on the curvature of this curve.

On the other hand, the simulations allow calculating directly the translational diffusion coefficient parallel to the layers $D_{\parallel}$ with equation 9. However, it was already shown that simulations are often not in quantitative agreement with experiments. For example, simulations performed with clayFF and both SPCE and TIP4P2005 water models were found to overestimate water diffusion coefficients in other types of clays.[23,26,44] It is also the case here, as shown on figure 4 where experimental and simulated $S_{\parallel}(Q,t)$ are compared.

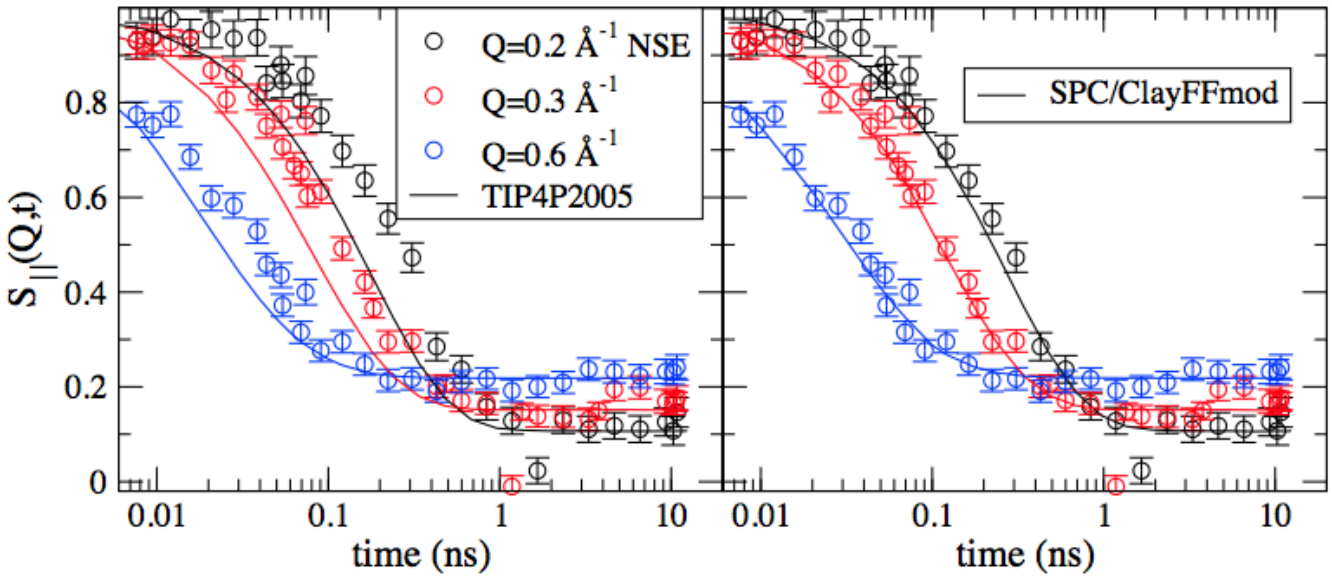

Figure 4: Comparison of experimental and simulated $S_{\parallel}(Q,t)$ having undergone the transformation of equation 14, at $T = 300$ K for TIP4P2005/clayFF (left) and SPC/clayFFmod (right). Black: Q=0.2 Å^{-1}, red: Q=0.3 Å^{-1}, blue: Q=0.6 Å^{-1}. Circles: NSE experiments.

Although both force fields overestimate the diffusion (the relaxation times are smaller than experimental ones), the flexible SPC with modified clayFF force-field gives much better agreement with experiment. Let us note that in this figure, simulated $S(Q,t)$ have undergone some transformations to be directly comparable with the experiments. Indeed, short-time dynamics, responsible for the factor A in equation 5 can be different between experiment and simulations: it depends on the water model and its accuracy to capture local water motions (for example, TIP4P2005 model is a rigid model and cannot account for vibrations). Moreover, simulated $S(Q,t)$ do not account for immobile clay hydrogens and the B value of the plateau must be added artificially to the simulated data. As a consequence, simulated

$S(Q,t)$ have been transformed so that the plateaus at very short times and very long times are the same as the experiment for each Q value. To do so, experimental and simulated $S(Q,t)$ were first fitted with equation 5 to get A_{exp}, B_{exp} and A_{sim} (B_{sim}=0). Then the following transformation was applied to $S_{sim}(Q,t)$:

$$S_{sim}^{new}(Q,t) = \frac{(A_{exp} - B_{exp})}{A_{sim}} S_{sim}(Q,t) + B_{exp} \tag{14}$$

As expected, S_{sim}^{new} given on figure 4 tend towards A_{exp} at short times and towards B_{exp} at high times. Thus the relaxation times can be directly compared.

In order to quantify now the differences in relaxation times between the experiment and the simulations, a further transformation was applied to simulated $S_{sim}^{new}(Q,t)$: the times were multiplied by a factor in order to shift the simulated points towards higher relaxation times, corresponding to a slower dynamics. Thus, the dynamics had to be slowed down by a factor 1.67 and 1.11 for TIP4P2005/clayFF and SPC/ClayFFmod respectively in order to fit the experimental $S(Q,t)$. The transformed $S_{sim}(Q,t)$ are given on figure 5 together with the experimental data. As soon as the simulated relaxation times are corrected, they fit remarkably well, which shows that the shapes of the experimental and simulated curves are very similar. As the diffusion coefficients obtained by MSD calculations (equation 9) are D=14.9$\times 10^{-10}$ m^2.s^{-1} and 9.87$\times 10^{-10}$ m^2.s^{-1} for TIP4P2005/clayFF and SPC/clayFFmod respectively, the multiplicative factors obtained on the relaxation times can be used to calculate undirectly the experimental parallel diffusion coefficient: $D_{exp} = D_{\mathrm{TIP4P}}/1.67 = D_{\mathrm{SPC}}/1.11 = 8.9.10^{-10}$ m^2.s^{-1}. It is not so far however above the error bar of both the value determined using jump diffusion (by 7%) and the value using the simple diffusion with Q=0.2 $\mathring{A}^{-1}$ (by 12 %). We underline that the simple models applied on the experimental value do not directly give $D_{\parallel}$ due to the mosaicity. According to Equation 7, which takes into account $D_{\perp}$ (lower than $D_{\parallel}$), D_{exp} underestimates $D_{\parallel}$ by less than 3%. D_{exp} estimated with MD is thus rather consistent with the experimental value.

Table 1 summerizes the values of the parallel diffusion coefficients obtained from NSE

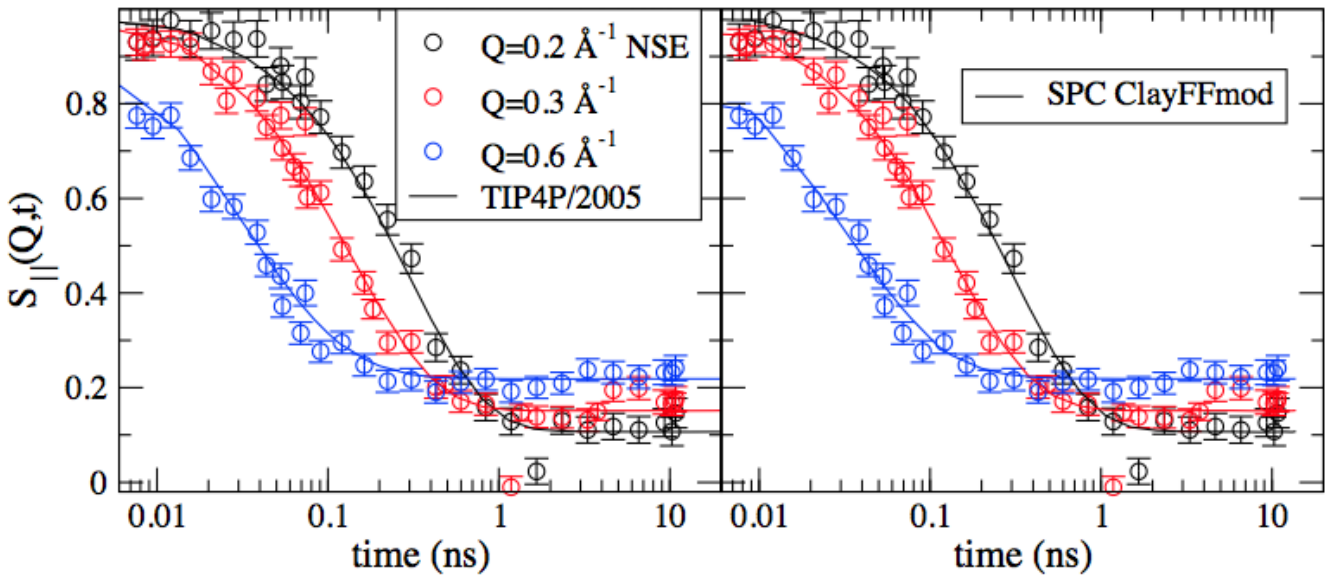

Figure 5: Comparison of experimental and transformed simulated $S_{\|}(Q,t)$ after the rescaling of the relaxation times, at T = 300K for TIP4P2005/clayFF (left) and SPC/clayFFmod (right). Black: Q=0.2 Å^{-1}, red: Q=0.3 Å^{-1}, blue: Q=0.6 Å^{-1}. Circles: NSE experiments.

and simulations. For the simulations, D_{bulk} is the diffusion coefficient of water corrected from the box size effect.[45] A formula exist to correct the diffusion coefficient calculated in slit pores from box size effects.[46] Even if its validity can be questioned in the case of very confined water, it was used to estimate the box size correction, which was found to be about 1% of the diffusion coefficient and was thus neglected.

Note that the value of 9.87×10^{-10} m^2.s^{-1} obtained for SPC/clayFFmod is about 30% higher than the value obtained by Michot et al.[25] with the same force field. This difference comes probably from the fact that their trajectories were much shorter (400 ps maximum), which can affect the statistics and the determination of diffusion coefficients at long time.

As SPC overestimates D_{bulk}, the characteristics of the slowing down of water in saponite compared with the bulk is analyzed with the ratio $D_{\|}/D_{bulk}$. It shows that water dynamics is more impacted by the presence of the clay in the case of SPC/ClayFFmod than both in the experiment, and with the simulations with TIP4P2005/clayFF.

Table 1: Diffusion coefficients in the clay $D_{\parallel}$, in the bulk D_{bulk} and ratio determined from the two types of simulations and NSE experiments.

	$D_{\parallel}$ (10^{-10} m^2.s^{-1})	D_{bulk} (10^{-10} m^2.s^{-1})	$D_{\parallel}/D_{bulk}$
TIP4P2005/clayFF	14.9	24.9 (ref[47])	0.60
SPC/clayFFmod	9.87	33.3	0.30
NSE experiment	8.9	24 (ref[48])	0.37

Diffusion perpendicular to the clay layers

$S_{\perp}(Q,t)$ should theoretically tend towards a plateau higher than the proportion of immobile clay hydrogen: this plateau should increase when Q decreases, which corresponds to the fact that at high distances of observation the bounded water H atoms are seen as immobile.[49] Because of the mosaicity of the sample however, measured $S_{\perp}(Q,t)$ are to some extent sensitive to the unbounded diffusion parallel to the clay layers. As a consequence, like $S_{\parallel}(Q,t)$, experimental $S_{\perp}(Q,t)$ decrease towards the proportion of immobile H constitutive of the clay layers (see figure 7). The influence of the parallel diffusion on the tail of $S_{\perp}(Q,t)$ is shown in the Figure S3 in SI as a function of Q and $\Delta\theta$. A more complex model than Equation 5 should therefore be used to fit $S_{\perp}(Q,t)$ in order to get meaningful fitting parameters. In addition, although equation 5 fitted $S_{\parallel}(Q,t)$ very well, it fits experimental $S_{\perp}(Q,t)$ very badly. Moreover, the estimation of the plateaus at small and high times is hazardous, thus it is not easy to transform $S_{\perp}(Q,t)$ to match the experimentla curves as closely as possible.

Hence, we found simpler to evaluate the sensitivity of $S_{\perp}(Q,t)$ to $D_{\perp}$ by using the two-diffusion model of equation 7 with the experimental value of $D_{\parallel}$ deduced in the previous section (89 Å^2/ps) and $\Delta\theta = 10°$. In the model, L=7.3 Å was taken as the width of the pore, evaluated from the H distributions calculated with TI4P2005/clayFF given on figure 10.

In figure 6, modelled $S_{\perp}(Q,t)$ at $Q = 0.6$ Å^{-1} are compared with experimental $S_{\perp}(Q,t)$ for several values of $D_{\perp}$. As the modelled $S_{\perp}(Q,t)$ start from 1 and go to 0 (no short time dynamics, no immobile H atoms), the modelled curves were transformed according to $S_{mod}^{new} = (A-B)S_{mod} + B$. For each curve from the model, A and B were calculated in order to minimize the difference between the whole set of modelled and experimental points, using

the least squares method. $D_\perp$ values have been chosen in order to vary the ratio $D_\perp/D_\parallel$ between 0 and 1.5, which clearly changes the shape of $S_\perp(Q,t)$.

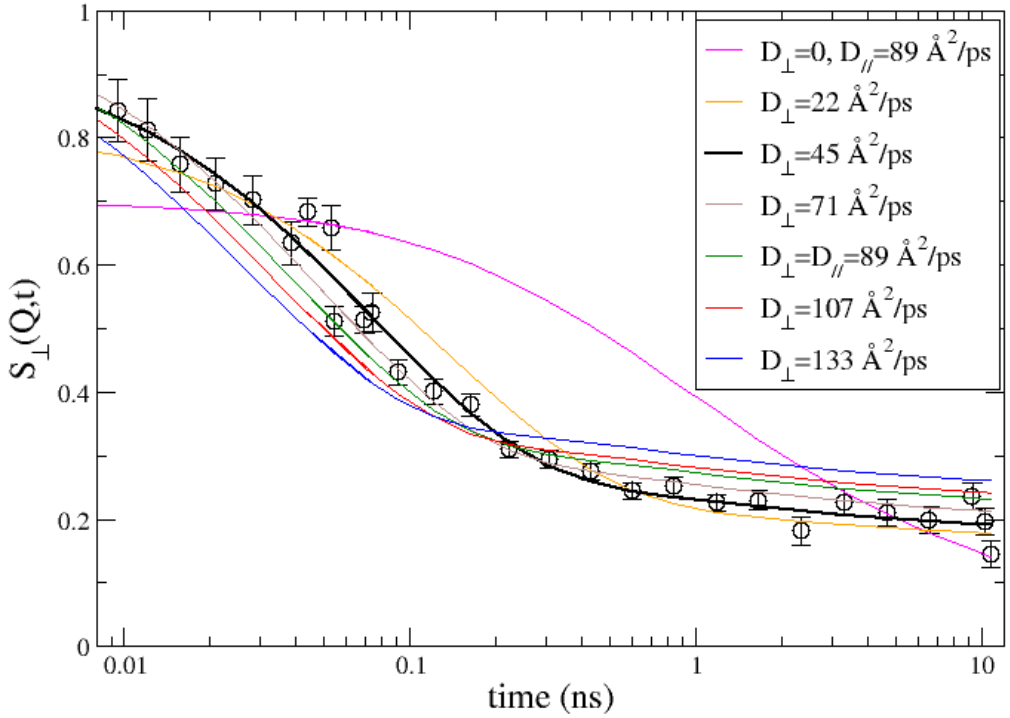

Figure 6: Comparison of experimental $S_\perp(Q,t)$ (circle) and the best transformed $S_\perp^{mod}(Q,t)$ (see text for details) for Q = 0.6 Å^{-1}, L=7.3 Å, $\Delta\theta$ = 10°, $D_\parallel$ = 8.9 × 10^{-10} m^2.s^{-1} and $D_\perp/D_\parallel$= 0, 0.25, 0.5, 0.8, 1.0, 1.2 and 1.5.

The best fit between modelled and experimental $S_\perp(Q,t)$ was obtained for $D_\perp/D_\parallel$=0.5, which means that the diffusion of water perpendicular to the clay layers is about half the parallel one. $D_\perp/D_\parallel$=0.8 is satisfactory but $D_\perp/D_\parallel$=0.5 is better. When $D_\perp$ is further increased, it is more and more difficult to fit at the same time the decreasing of $S_\perp(Q,t)$ and the value of the plateau at high times (blue curve). As a result, the relaxation times become too small. On the other hand, when $D_\perp$ is too small, it is more and more difficult to fit at the same time the decreasing of $S_\perp(Q,t)$ and the value of the plateau at small times (pink curve). As a result, the relaxation times become too high. Let us note that $D_\perp/D_\parallel$=0.5

also provides very good agreement between experimental data and the model for Q = 1.0 Å^{-1} (figure 7). The agreement is less good for Q=1.2 Å^{-1} but the experiment is very noisy and for high values of Q, describing the motions of HW by a simple translational diffusion becomes a risky simplification.

Finally, we checked that changing the mosaicity $\Delta\theta$ by $\pm 5°$ and L by 0.3 Å (L=7 Å is found by analyzing the H densities with SPC/clayFFmod, see figure 10) did not alter the results of the fits and the final value for the best agreement between model and experiment: $D_\perp/D_\parallel$=0.5.

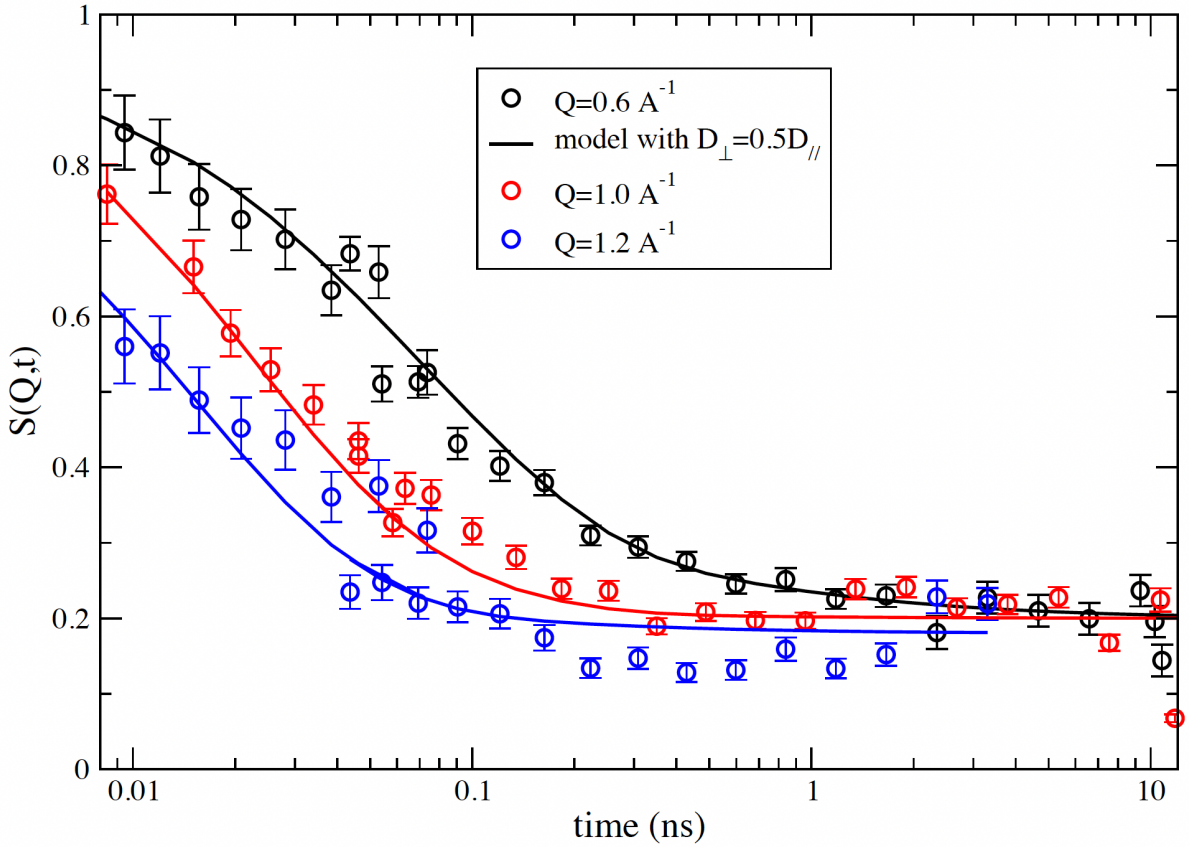

Figure 7: Comparison of experimental and modelled $S_\perp(Q,t)$ with $D_\perp/D_\parallel$=0.5 at T=300K. Black: $Q = 0.6$ Å^{-1}, red: $Q = 1.0$ Å^{-1}, blue: $Q = 1.2$ Å^{-1}. Solid line: model, circles: NSE experiments.

Along with this analysis, $D_\perp$ was calculated from simulations according to equation 10. As autocorrelation functions of Ψ are rather noisy after 250 ps, $D_\perp$ was calculated from the

linear part of the correlation function between 100 and 200 ps (see Figure S4 in SI). From the H densities along z (Figure 10), values of 7.0 Å and 7.3 Å were taken for L in SPC and TIP4P2005 cases respectively. The determined $D_\perp$ were found to be equal to $5.2.10^{-10}$ and $7.4.10^{-10}$ $m^2.s^{-1}$ for SPC/clayFFmod and TIP4P2005/clayFF force fields respectively. It corresponds to ratios $D_\perp/D_\parallel$=0.53 and 0.50, that both agree very well with the value given by the model fitted on experimental data. In conclusion, the slowing down of water diffusion in the direction perpendicular to the clay layers compared to the diffusion parallel to the layers is the same for experiments and simulations.

Evolution with temperature

Experimental $S(Q,t)$ were analyzed in the same way for the temperatures T=255 and 350 K. Simulated $S_\parallel(Q,t)$ were transformed to retrieve experimental plateaus at small and high times. They are given on figure 8.

At T = 255K, both force fields overestimate the dynamics, but SPC/clayFFmod is in much better agreement than TIP4P2005/clayFF. The calculated $D_\parallel$ obtained from MSD calculations give $D = 4.83 \times 10^{-10}$ and 2.32×10^{-10} $m^2.s^{-1}$ for TIP4P2005/clayFF and SPC/clayFFmod respectively. Then the dynamics had to be slowed down by a factor 3.12 and 1.50 to retrieve experimental $S_\parallel(Q,t)$ (see Figure S5 in SI). Hence parallel D_{exp} can be estimated by $D_{exp} = D_{\mathrm{TIP4P}}/3.12 = D_{\mathrm{SPC}}/1.50 = 1.55 \times 10^{-10}$ $m^2.s^{-1}$.

At T = 350K, TIP4P2005/clayFF overestimate the water diffusion, although SPC/clayFFmod underestimates it. MSD calculations give $D = 30.1 \times 10^{-10}$ and 23.7×10^{-10} $m^2.s^{-1}$ for TIP4P2005/clayFF and SPC/clayFFmod respectively, and the multiplicative factors were found to be 1.13 and 0.89, leading to $D_{exp} = D_{\mathrm{TIP4P}}/1.13 = D_{\mathrm{SPC}}/0.89 = 26.5 \times 10^{-10}$ $m^2.s^{-1}$.

All these diffusion coefficients are reported in table 2 for the three temperatures. Activation energies were obtained from the slope of $\ln D$ as a function of $1/T$ (see Figure S6 in SI).

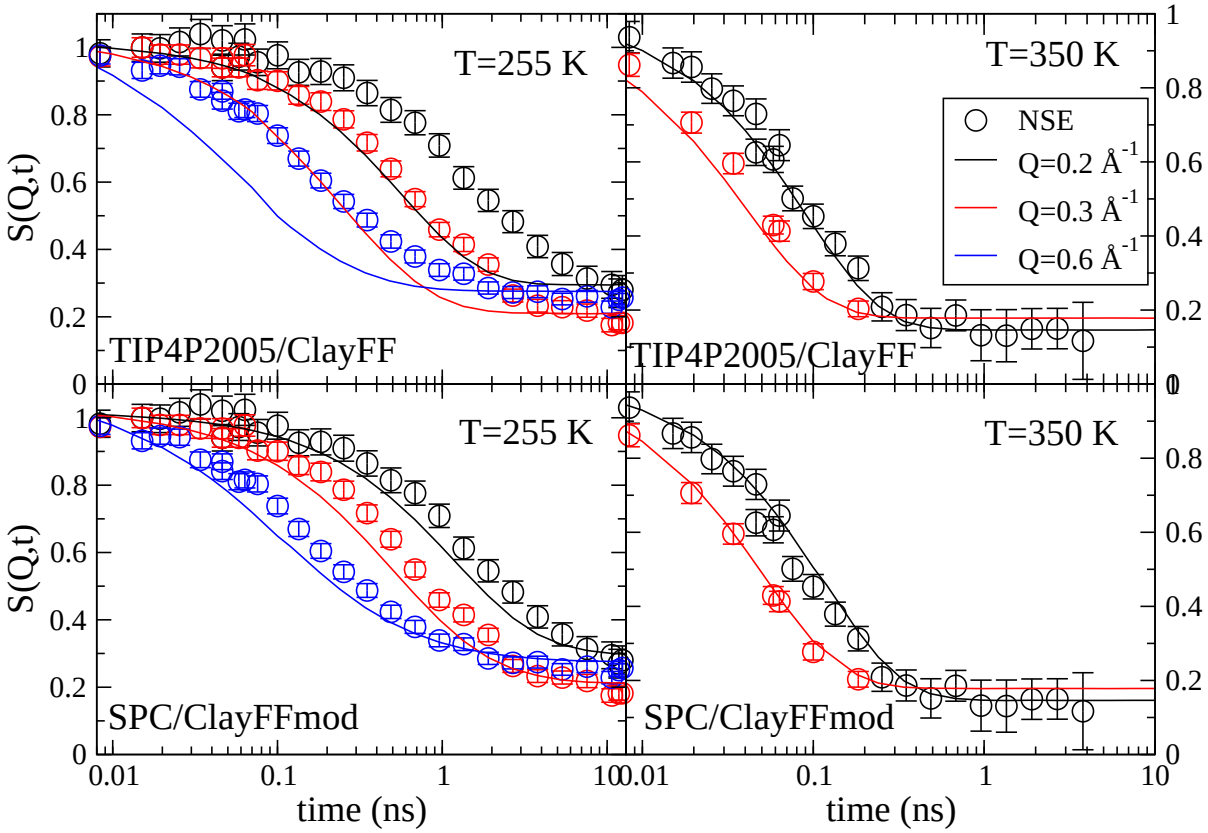

Figure 8: Comparison of experimental and transformed simulated $S_{\|}(Q,t)$ at T=255 K (left) and T=350 K (right) with TIP4P2005/clayFF (top) and SPC/ClayFFmod (bottom). Black: $Q = 0.2$ Å^{-1}, red: $Q = 0.3$ Å^{-1}, blue: $Q = 0.6$ Å^{-1}. Solid line: simulations, circles: NSE experiments.

To conclude on the diffusion parallel to the clay layers, TIP4P2005/clayFF is in worse agreement with experiment than SPC/clayFFmod, except for T=350 K. The activation energies must be compared to the ones obtained in bulk water. The latter were calculated in the range of temperature [270 K,350 K] where water is expected to be liquid. Indeed, at lower temperatures, supercooled water has been studied however its behaviour differs from bulk water.[50] Anyway, although flexible SPC water gives for bulk water D and E_a much further from real value than TIP4P/2005, the shift $\Delta E_a = E_a - E_a(\text{bulk})$ is much closer to

the experimental value. This is not the case with TIP4P2005/clayFF for which a negative ΔE_a has been calculated.

Table 2: $D_{\parallel}$ (10^{-10} m^2.s^{-1}) at the three temperatures measured in the NSE experiments, both calculated and measured; Activation energy E$_a$ (kJ/mol) for the clay and for the bulk, as well as the shift ΔE_abetween both (kJ/mol).

	$D_{\parallel}$ 255 K	$D_{\parallel}$ 300 K	$D_{\parallel}$ 350 K	E_a (clay)	E_a(bulk)	ΔE_a
TIP4P2005/clayFF	4.83	14.9	30.1	14.3	17.4	-3.1
SPC/clayFFmod	2.32	9.87	23.7	18.2	13.5	4.7
NSE experiment	1.55	8.9	26.5	22.3	17.6	4.7

$D_{\perp}$ were calculated at $T = 255$ K using equation 10. The ratio $D_{\perp}/D_{\parallel}$ was found to be equal to 0.33 and 0.39 for TIP4P2005/clayFF and SPC/clayFFmod respectively. These ratios were used to calculate $S_{\perp}(Q,t)$ with the two-diffusion model, that were compared with experiment. As seen on figure 9, the model with the simulated $D_{\perp}/D_{\parallel}$ is in good agreement with experiment, with a slightly better agreement with the ratio 0.39 found with SPC/clayFFmod for $Q = 0.6$ Å^{-1}.

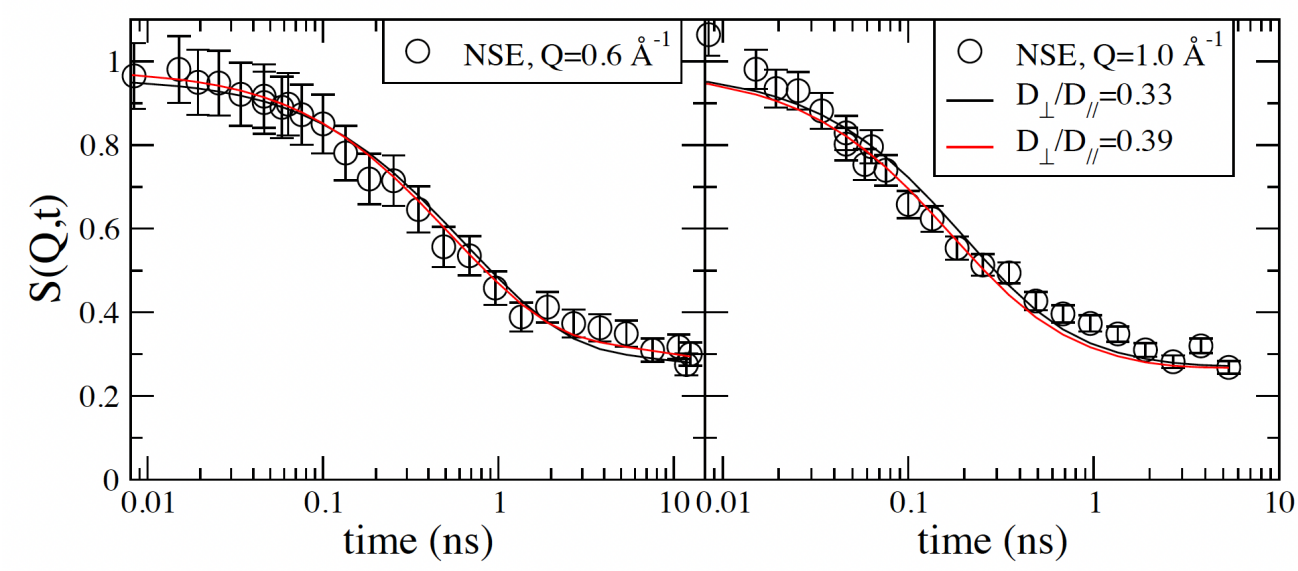

Figure 9: Comparison of experimental and modelled $S_{\perp}(Q,t)$ at T=255 K at $Q = 0.6$ Å^{-1} (left) and $Q = 1.0$ Å^{-1} (right) for $D_{\perp}/D_{\parallel}$=0.33 (black line) and $D_{\perp}/D_{\parallel}$=0.39 (red line). Circles: NSE experiments.

An activation energy for D$_{\perp}$ can be calculated from these two temperatures. The result

are 21.8 kJ/mol and 24.7 kJ/mol for TIP4P2005/clayFF and SPC/clayFFmod respectively, that is to say about 7 kJ/mol higher than activation energies found for $D_{\parallel}$ whatever the force field. It is not surprising considering the electric fields perpendicular to the clay layers generated by the negative charge of the surfaces, which orientate the water molecules with their H towards the surface. In order to diffuse along the z direction, a water molecule must overcome the action of this field, which is added to the other interactions, between water molecules among others.

Discussion

The analysis of the experimental data in the light of the results given by molecular simulations allowed us to calculate diffusion coefficients of water in bihydrated saponite for several temperatures. The comparison with the simulated data leads to the conclusion that SPC/ClayFFmod force field is in much better agreement with neutron data, even if the ratios $D_{\perp}/D_{\parallel}$ are close for both force fields.

In this section, we are more interested in explaining the evolution of the parallel diffusion coefficients with temperature on the basis of the differences observed between both force fields.

Despite the two water models which are different, the difference between the two force fields is the size of the surface oxygen atoms which has been increased by 7 % in clayFFmod. As a result, the fluid atoms are a bit more repelled from the surface, as seen on the atomic OW distributions of figure 10, and then a little more confined, what could possibly contribute to a slight decrease of the dynamics. However the main difference between the distributions concerns sodium cations: although they are mostly completely hydrated in the case of SPC/clayFFmod, they mostly stick to the surface in the case of TIP4P2005/clayFF, attracted by the negative substitutions located at the surface of the clay. As a consequence the self-diffusion of sodium cations is four times less with TIP4P2005/clayFF force field

(5.0×10^{-11} $m^2.s^{-1}$) than with SPC/clayFFmod (2.0×10^{-10} $m^2.s^{-1}$).

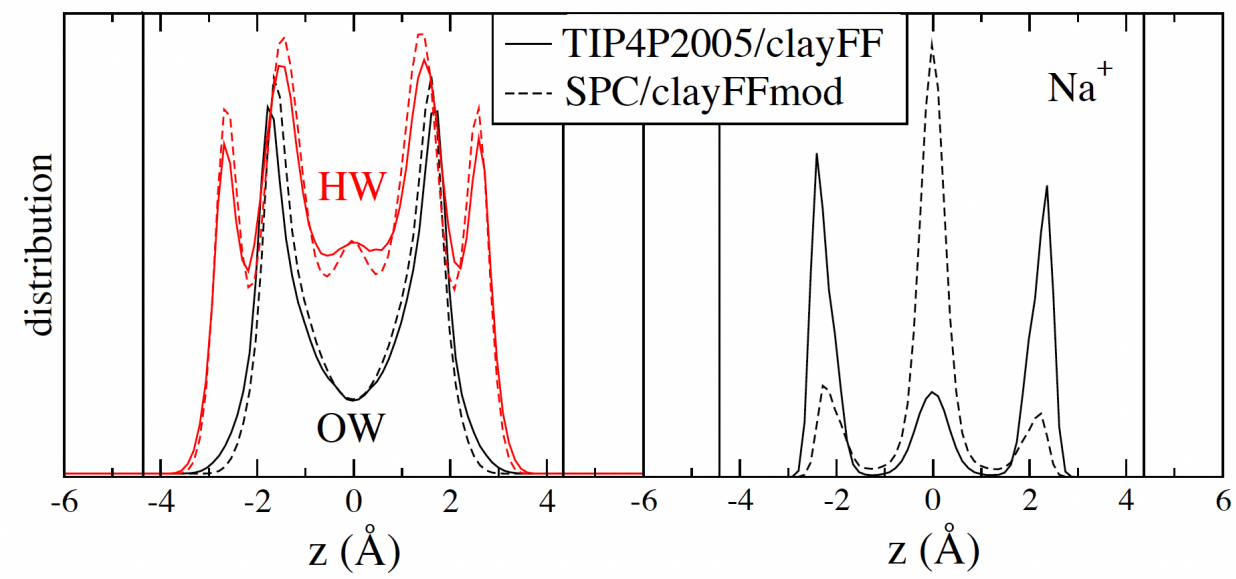

Figure 10: Distributions of mobile species in saponite interlayers. Left: water atoms (OW in black, HW in red). Right: Na^+ atoms. Solid lines: TIP4P2005/clayFF force field, dashed lines: SPC/ClayFFmod force field. The positions of the oxygen surface atoms are indicated by vertical black solid lines.

In order to study in more detail the effect of cations on water dynamics, we analyzed molecular dynamics parallel to the clay layers by differentiating water molecules inside and outside cation hydration spheres. To do so, radial distribution functions g_{NaOW} between sodium ions and water oxygens were calculated. Following the methodology proposed in ref,[51] we were able to calculate the residence time of water molecules inside (τ_0 for state 0, "bonded") and outside (τ_1 for state 1, "free") cations hydration spheres. These times are the characteristic decays of the presence probabilities $P_i(t)$ plotted in Figure 11. They are close for both force fields (τ_0=47 or 60 ps; τ_1=83 or 95 ps), which is consistent with the rather similar cation/water interaction for both force fields. We can check that the fraction of time spent by a water molecule in state 0 ($\frac{\tau_0}{\tau_0+\tau_1} = 0.39$ for SPC/ClayFFmod and 0.36 for TIP4P2005/clayFF) is approximately equal to the proportion of water molecules in that state on average. Indeed the average over the trajectories gives a population of "bonded" water molecules equal to $\frac{N_0}{N_0+N_1} = 0.42$ and 0.38 for SPC/ClayFFmod and TIP4P2005/clayFF

respectively. Over the timescale of the decay of the $P_i(t)$ functions, it was therefore possible to determine diffusion coefficients from the calculated parallel mean-squared displacements as a function of time t for the molecules staying in state 1 during time t (see SI for methodology details). Given that N_0 and N_1 are greater than a thousand molecules, the estimation of the MSD remains statistically satisfactory, even when $P_i(t)$ are divided by 10, which explains the observed clean linear evolution of MSD_1 up to $t = 200$ ps. Therefore, diffusion coefficients for water molecules outside the hydration sphere of cations (state 1) could be calculated on the linear part of $MSD_1(t)$, between 100 and 200 ps. They are given in the table 3 and commented later in the text.

As seen on figure 11 however, it is not possible to properly calculate a self-diffusion for "bonded" water molecules from $MSD_0(t)$ because MSD_0 bends with time. It can be compared to the MSD of the cations (inset of Figure 11). The bonded water molecules should diffuse as the cations on long timescales, which appears reasonable in the range 150-200 ps with SPC/ClayFFmod, while the diffusion of water appears quicker than the one of cations with TIP4P2005/clayFF. The timescale may nevertheless be too short however MSD cannot be calculated beyond 200 ps due to the bad statistics in this regime. On the short times, faster water molecules could increase MSD's slope before leaving the hydration sphere, i.e. state 0. Moreover the small value of MSD_0 reached at 200 ps (less than 8 $Å^2$) can also represent local moves, like the ones of water confined within the hydration sphere of an immobile cation adsorbed to a tetrahedral substitution of the surface. Although precise quantitative conclusions are difficult to draw for state 0, it can be concluded that the diffusion of these water molecules is tightly linked to the one of the cations.

The strong effect of the adsorbed cations on water dynamics can be confirmed by comparing simulated data obtained with the same force field, TIP4P2005/clayFF, for two different clays, saponite and hectorite. The hectorite formula is $Si_8Mg_{5.2}Li_{0.8}O_{20}(OH)_4Na_{0.8}n_{H_2O}$ for the half unit cell. The only difference with saponite is the location of the negative substitutions: they are located at the tetrahedral sheet for saponite (Si^{4+} is replaced by Al^{3+}),

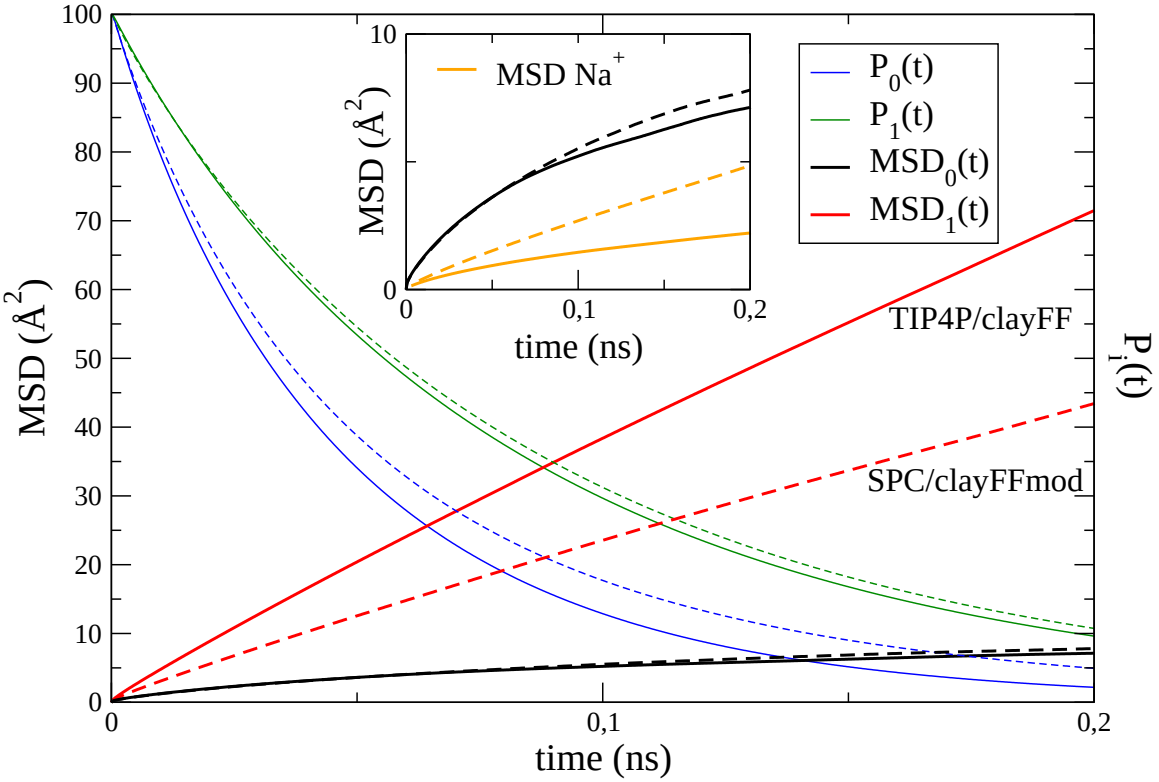

Figure 11: Presence probabilities $P_i(t)$ (in percents) and parallel mean-squared displacements $\mathrm{MSD}_i(t) = \frac{\langle x^2+y^2 \rangle}{2}$ of water molecules belonging (state 0) or not belonging (state 1) to cation hydration spheres. Blue: $P_0(t)$, green: $P_1(t)$, black: $\mathrm{MSD}_0(t)$, red: $\mathrm{MSD}_1(t)$, yellow: MSD of Na^+, Solid line: TIP4P2005/clayFF force field, dashed line: SPC/ClayFFmod force field.

and in the octahedral sheet of the clay layer for hectorite (Mg^{2+} is replaced by Li^+). The substitutions are thus in the middle of the sheets for hectorite and closer to their surfaces for saponite. The negative substitution being further from the fluid in the case of hectorite, cations are less attracted by the surface and then fully hydrated (see Figure S8 in SI). Comparison between the two clays makes it possible to study the effect of the location of the cations, by overcoming the difference in force fields. $\mathrm{MSD}_0(t)$ and $\mathrm{MSD}_1(t)$ are plotted for the two clays on figure 12.

Unlike saponite, the linear evolution of $\mathrm{MSD}_0(t)$ in hectorite allows to calculate a diffusion

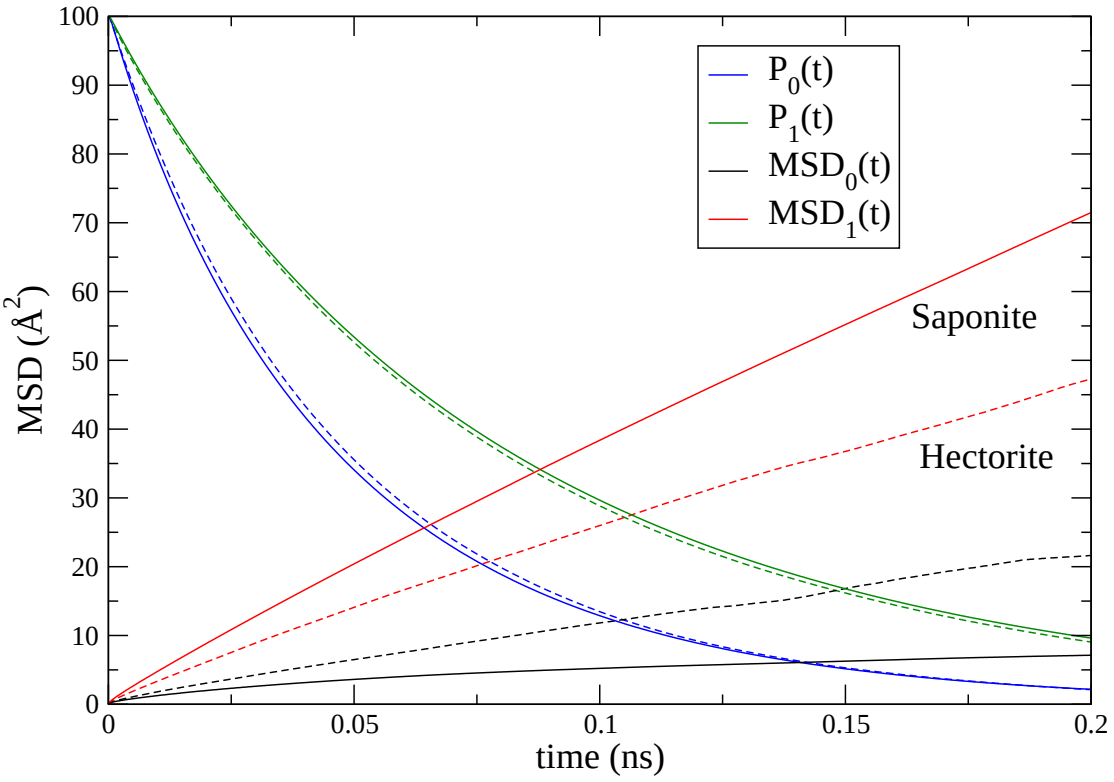

Figure 12: Presence probabilities $P_i(t)$ (in percents) and parallel mean-squared displacements $\mathrm{MSD}_i(t)$ of water molecules belonging (state 0) or not belonging (state 1) to cation hydration spheres. Blue: $P_0(t)$, green: $P_1(t)$, black: $\mathrm{MSD}_0(t)$, red: $\mathrm{MSD}_1(t)$. Solid line: Saponite, dashed line: Hectorite. In both cases, the force field used is TIP4P2005/clayFF.

coefficient for "bonded" water molecules from the slope of the linear part of $\mathrm{MSD}_0(t)$: one finds $D_0 = 5.4 \times 10^{-10}$ m^2.s^{-1}, which is very close to the diffusion coefficient of Na^+, 5.2 $\times 10^{-10}$ m^2.s^{-1}. We can see that the model works well in this case, probably because only one rather mobile population of Na^+ is present in hectorite, whereas two types of cations in saponite give rise to several populations of waters as well, which complicates the analysis. The development of a model separating, within state 0, molecules linked to mobile cations and immobile cations would make it possible to refine the interpretation. Nevertheless, given the close link between the behavior of "bonded" water and that of cations, we believe that

the study of "free" water on the one hand and that of cations on the other, already gives us valuable information for exploring activation energies.

Looking at water molecules in state 1 now, we see on figure 11 that they diffuse much faster in saponite with TIP4P2005/clayFF than with SPC/clayFFmod: the self-diffusion coefficient obtained from the slope of $MSD_1(t)$ is 23 $\times 10^{-10}$ $m^2.s^{-1}$ with TIP4P2005/clayFF (very close to the bulk value) and 15 $\times 10^{-10}$ $m^2.s^{-1}$ with SPC/clayFFmod. As a consequence the average water diffusion coefficient is higher with the former force field than with the latter as shown in the previous section.

Here again, comparison with hectorite is useful to understand the origin of these differences. Although the force field is the same (TIP4P2005/clayFF), water molecules in state 1 diffuse significantly slower in hectorite ($D_1 = 12 \times 10^{-10}$ $m^2.s^{-1}$) than in saponite ($D = 23 \times 10^{-10}$ $m^2.s^{-1}$). The fact that the majority of the counterions are adsorbed on the surface of saponite seems to play a crucial role on dynamics of "free" molecules. Several explanations can be found: 1) The cations adsorbed on the surface in saponite hide the negative charge of the clay surface, then water molecules are less polarized by the surface/ have less interactions with the surface. 2) The cations located in the middle of the interlayer space in hectorite act like obstacles that disrupt the H-Bond network and slows down the diffusion of "free" water molecules.

A calculation of the average number of hydrogen bonds formed with the clay surface (with the criterion used by Luzar and Chandler[52]) showed that about 43 % of the water molecules in saponite form one H-bond with the surface, versus 49 % in hectorite. Although this difference could partly explain the slowing down in hectorite, a detailed study of the strength of these H-bonds could help and it is probable that the diffusion process of "free" water molecules is significantly changed by the location of the cations too.

Diffusion coefficients of cations and "free" water molecules (state 1) in saponite are reported in table 3 for the three studied temperatures for both force fields, together with the activation energies.

Table 3: Diffusion coefficients of the cations $D_{\|}(Na^+)$ and of the free water molecules D_1 (water in state 1) in saponite calculated with the two force fields at different temperatures. The resulting activation energies are given.

Temperature	255 K	300 K	350 K	
	$D_{\|}(Na^+)$ (10^{-10} $m^2.s^{-1}$)			E_a (kJ/mol)
TIP4P2005/clayFF	0.12	0.50	1.35	18.9
SPC/clayFFmod	0.38	2.0	5.7	21.2
	D_1 (10^{-10} $m^2.s^{-1}$)			E_a (kJ/mol)
TIP4P2005/clayFF	9.66	23.1	40.2	11.2
SPC/clayFFmod	4.68	14.8	29.5	14.4

For SPC/clayFFmod, E_a of "free" water molecules (14.4 kJ/mol) is a bit higher than E_a of bulk water (13.5 kJ/mol). Counterions have a much higher activation energy. As stated in previous work,[26] the higher activation energy of the whole water in the intelayer space is then mostly due to the water molecules located in the hydration spheres of the cation. For TIP4P2005/clayFF, the activation of "free" water molecules is very low compared to the bulk one (11.2 kJ/mol versus 17.4 kJ/mol). It explains why the activation energy of water is on average lower in saponite than in the bulk despite the higher activation energy of the cations. The diffusion mechanism and its activation energy being mostly related to the H-bonds network rearrangements,[35] we calculated the total number of hydrogen bonds formed by "free" water molecules with other water molecules and surfaces. We assume that the more and the stronger H-bonds a water molecule forms, the more difficult will be its diffusion. In fact, the number of H-bonds formed with other molecules was found to be very similar for both force fields. Moreover, around 20 % more hydrogen bonds were found between "free" water molecules and the surface with TIP4P2005/ClayFF, which goes in the opposite direction of our assumption. Hence, no clear explanation appears for this low activation energy. A more detailed study of the dynamics of hydrogen bonds according to the type of water (bonded/free) and of their strength could probably allow to explain these differences.[35] The activation energies of the different interactions contributing to water diffusion could be calculated using ref[53] which could help to explain the discrepancies between the force fields and to better define the origin of the higher experimental activation energy.

Conclusion

Water dynamics has been studied in an anisotropic confining medium constituted by the bilayer state of a swelling saponite synthetic clay. Water is thus confined between two negatively charged planes surrounded by sodium cations. Thanks to the use of a macroscopically oriented film of clay, the dynamics of water has been analyzed perpendicular and parallel to the solid/liquid interfaces. Neutron Spin Echo (NSE) experiments are associated with Molecular Dynamics (MD) simulations in order to extract information linked to the role of cations, the dynamics of which on these time and length scales can only be calculated. Two sets of force fields have been used for water and clays in MD calculations.

The experimental and calculated diffusion coefficients paralell to the clay planes ($D_{\parallel}$) can be directly compared. The best agreement is obtained with the calculations done with SPC model for water and modified ClayFF for the clay[24] whatever the temperature between 255 K and 350 K. The slowing down in the diffusion coefficient perpendicular to the clay layers ($D_{\perp}$) is also in good agreement between these simulations and the experiments.

For both force fields used, (i) the water around the cations is slowed down more than water outside the hydration spheres, (ii) this type of water is responsible for the increase in the activation energy of the diffusion processes, (iii) the diffusion of water around the Na^+ cation is similar. In contrast, the location of the cations in the interlayer space differs and this seems to have the most important impact on water dynamics. The hydrated cations located in the middle of the interlayer space seem to constitute obstacles that inhibit "free" water diffusion more than when they are located close to the surface. Further investigations are needed to calculate the individual contributions of the different energy terms (Lennard-Jones, electrostatic, kinetic energy) to the overall activation energy of the diffusion process.[53]

Supplementary information

This file contains additional figures and detailed explanations on model and simulations.

Acknowledgments

We thank ILL for the beamtime attributed on IN15 and for the support provided during the experiments. This work was granted access to the HPC resources of IDRIS under the allocation 2021-A0100412473 made by GENCI. The authors are grateful to the CNRS interdisciplinary "défi Needs" program (Project DARIUS).

References

(1) Brovchenko, I.; Oleinikova, A. *Interfacial and confined water*; Elsevier, 2008; pp 1–149.

(2) Cerveny, S.; Mallamace, F.; Swenson, J.; Vogel, M.; Xu, L. Confined water as model of supercooled water. *Chem. Rev.* **2016**, *116*, 7608–7625.

(3) Michot, L. J.; Villiéras, F.; François, M.; Bihannic, I.; Pelletier, M.; Cases, J.-M. Water organisation at the solid–aqueous solution interface. *Compt. Rendus Geosci.* **2002**, *334*, 611–631.

(4) Wang, D.; Tian, Y.; Jiang, L. Abnormal Properties of Low-Dimensional Confined Water. *Small* **2021**, *17*, 2100788.

(5) Zhu, H.; Wang, Y.; Fan, Y.; Xu, J.; Yang, C. Structure and Transport Properties of Water and Hydrated Ions in Nano-Confined Channels. *Advanced Theory and Simulations* **2019**, *2*, 1900016.

(6) Biswas, R.; Bagchi, B. Anomalous water dynamics at surfaces and interfaces: synergistic effects of confinement and surface interactions. *Journal of Physics: Condensed Matter* **2018**, *30*, 013001.

(7) Tsimpanogiannis, I. N.; Moultos, O. A.; Franco, L. F. M.; Spera, M. B. D. M.; Erdős, M.; Economou, I. G. Self-diffusion coefficient of bulk and confined water: a

critical review of classical molecular simulation studies. *Molecular Simulation* **2019**, *45*, 425–453.

(8) Aluru, N. R.; Aydin, F.; Bazant, M. Z.; Blankschtein, D.; Brozena, A. H.; De Souza, J. P.; Elimelech, M.; Faucher, S.; Fourkas, J. T.; Koman, V. B. et al. Fluids and Electrolytes under Confinement in Single-Digit Nanopores. *Chemical Reviews* **2023**, *123*, 2737–2831.

(9) Wang, M.; Hou, Y.; Yu, L.; Hou, X. Anomalies of Ionic/Molecular Transport in Nano and Sub-Nano Confinement. *Nano Letters* **2020**, *20*, 6937–6946.

(10) Xue, M.; Qiu, H.; Shen, C.; Zhang, Z.; Guo, W. Ion Hydration under Nanoscale Confinement: Dimensionality and Scale Effects. *The Journal of Physical Chemistry Letters* **2022**, *13*, 4815–4822.

(11) Won, C. Y.; Aluru, N. Structure and dynamics of water confined in a boron nitride nanotube. *J. Phys. Chem. C* **2008**, *112*, 1812–1818.

(12) Falk, K.; Sedlmeier, F.; Joly, L.; Netz, R. R.; Bocquet, L. Molecular origin of fast water transport in carbon nanotube membranes: superlubricity versus curvature dependent friction. *Nano Lett.* **2010**, *10*, 4067–4073.

(13) Li, Q.; Song, J.; Besenbacher, F.; Dong, M. Two-dimensional material confined water. *Accounts of chemical research* **2015**, *48*, 119–127.

(14) Bañuelos, J. L.; Borguet, E.; Brown, G. E.; Cygan, R. T.; DeYoreo, J. J.; Dove, P. M.; Gaigeot, M.-P.; Geiger, F. M.; Gibbs, J. M.; Grassian, V. H. et al. Oxide– and Silicate–Water Interfaces and Their Roles in Technology and the Environment. *Chemical Reviews* **2023**, *123*, 6413–6544.

(15) Clark, G.; Grim, R.; Bradley, W. A study of the behavior of montmorillonite upon wetting. *Z. Kristallogr. Cryst. Mater* **1937**, *97*, 216–222.

(16) Norrish, K. The swelling of montmorillonite. *Discuss. Faraday Soc.* **1954**, *18*, 120–134.

(17) Porion, P.; Asaad, A.; Dabat, T.; Dazas, B.; Delville, A.; Ferrage, E.; Hubert, F.; Jimenez-Ruiz, M.; Michot, L. J.; Savoye, S. et al. Water and Ion Dynamics in Confined Media: A Multi-Scale Study of the Clay/Water Interface. *Colloids Interfaces* **2021**, *5*.

(18) Wang, G.; Ran, L.; Xu, J.; Wang, Y.; Ma, L.; Zhu, R.; Wei, J.; He, H.; Xi, Y.; Zhu, J. Technical development of characterization methods provides insights into clay mineral-water interactions: A comprehensive review. *App. Clay Sci.* **2021**, *206*, 106088.

(19) Nair, A. K. N.; Cui, R.; Sun, S. Overview of the Adsorption and Transport Properties of Water, Ions, Carbon Dioxide, and Methane in Swelling Clays. *ACS Earth Space Chem.* **2021**, *5*, 2599–2611.

(20) Ma, Z.; Gamage, R. P.; Rathnaweera, T.; Kong, L. Review of application of molecular dynamic simulations in geological high-level radioactive waste disposal. *App. Clay Sci.* **2019**, *168*, 436–449.

(21) Mitra, S.; Sharma, V. K.; Mukhopadhyay, R. Diffusion of confined fluids in microporous zeolites and clay materials. *Rep. Prog. Phys.* **2021**, *84*, 066501.

(22) Michot, L. J.; Delville, A.; Humbert, B.; Plazanet, M.; Levitz, P. Diffusion of water in a synthetic clay with tetrahedral charges by combined neutron time-of-flight measurements and molecular dynamics simulations. *J. Phys. Chem. C* **2007**, *111*, 9818–9831.

(23) Marry, V.; Dubois, E.; Malikova, N.; Durand-Vidal, S.; Longeville, S.; Breu, J. Water dynamics in hectorite clays: Infuence of temperature studied by coupling neutron spin echo and molecular dynamics. *Environ. Sci. Technol.* **2011**, *45*, 2850–2855.

(24) Ferrage, E.; Sakharov, B. A.; Michot, L. J.; Delville, A.; Bauer, A.; Lanson, B.; Grangeon, S.; Frapper, G.; Jiménez-Ruiz, M.; Cuello, G. J. Hydration Properties and Interlayer Organization of Water and Ions in Synthetic Na-Smectite with Tetrahedral

Layer Charge. Part 2. Toward a Precise Coupling between Molecular Simulations and Diffraction Data. *J. Phys. Chem. C* **2011**, *115*, 1867–1881.

(25) Michot, L. J.; Ferrage, E.; Jiménez-Ruiz, M.; Boehm, M.; Delville, A. Anisotropic features of water and ion dynamics in synthetic Na- and Ca-smectites with tetrahedral layer charge. A combined quasi-elastic neutron-scattering and molecular dynamics simulations study. *J. Phys. Chem. C* **2012**, *116*, 16619–16633.

(26) Marry, V.; Dubois, E.; Malikova, N.; Breu, J.; Haussler, W. Anisotropy of water dynamics in clays: Insights from molecular simulations for experimental QENS analysis. *J. Phys. Chem. C* **2013**, *117*, 15106–15115.

(27) Dazas, B.; Lanson, B.; Delville, A.; Robert, J.-L.; Komarneni, S.; Michot, L. J.; Ferrage, E. Influence of tetrahedral layer charge on the organization of interlayer water and ions in synthetic Na-saturated smectites. *J. Phys. Chem. C* **2015**, *119*, 4158–4172.

(28) Michot, L.; Bihannic, I.; Pelletier, M.; Rinnert, E.; Robert, J. Hydration and swelling of synthetic Na-saponites: Influence of layer charge. *Am. Min.* **2005**, *90*, 166–172.

(29) Ferrage, E.; Lanson, B.; Michot, L. J.; Robert, J.-L. Hydration Properties and Interlayer Organization of Water and Ions in Synthetic Na-Smectite with Tetrahedral Layer Charge. Part 1. Results from X-ray Diffraction Profile Modeling. *J. Phys. Chem. C* **2010**, *114*, 4515–4526.

(30) Dabat, T.; Hubert, F.; Paineau, E.; Launois, P.; Laforest, C.; Grégoire, B.; Dazas, B.; Tertre, E.; Delville, A.; Ferrage, E. A general orientation distribution function for clay-rich media. *Nat. Commun.* **2019**, *10*, 5456.

(31) Malikova, N.; Cadènea, A.; Dubois, E.; Marry, V.; Durand-Vidal, S.; Turq, P.; Breu, J.; Longeville, S.; Zanotti, J. M. Water diffusion in a synthetic hectorite clay studied by quasi-elastic neutron scattering. *J. Phys. Chem. C* **2007**, *111*, 17603–17611.

(32) Bée, M. *Quasielastic neutron scattering : principles and applications in solid state chemistry, biology, and materials science*; Adam Hilger, Bristol (UK), 1988; p 272.

(33) Laage, D. Reinterpretation of the Liquid Water Quasi-Elastic Neutron Scattering Spectra Based on a. *J. Phys. Chem. B* **2009**, *113*, 2684–2687.

(34) Malikova, N.; Cadène, A.; Marry, V.; Dubois, E.; Turq, P. Diffusion of water in clays on the microscopic scale: Modeling and experiment. *J. Phys. Chem. B* **2006**, *110*, 3206–3214.

(35) Gomez, A.; Piskulich, Z. A.; Thompson, W. H.; Laage, D. Water Diffusion Proceeds via a Hydrogen-Bond Jump Exchange Mechanism. *J. Phys. Chem. Lett.* **2022**, *13*, 4660–4666.

(36) Petersen, M. H.; Vernet, N.; Gates, W. P.; Villacorta, F. J.; Ohira-Kawamura, S.; Kawakita, Y.; Arai, M.; Kneller, G.; Bordallo, H. N. Assessing Diffusion Relaxation of Interlayer Water in Clay Minerals Using a Minimalist Three-Parameter Model. *J. Phys. Chem. C* **2021**, *125*, 15085–15093.

(37) Marry, V.; Malikova, N.; Cadène, A.; Dubois, E.; Durand-Vidal, S.; Turq, P.; Breu, J.; Longeville, S.; Zanotti, J. M. Water diffusion in a synthetic hectorite by neutron scattering - Beyond the isotropic translational model. *J. Phys. Condens. Matter* **2008**, *20*.

(38) Cygan, R. T.; Liang, J. J.; Kalinichev, A. G. Molecular models of hydroxide, oxyhydroxide, and clay phases and the development of a general force field. *J. Phys. Chem. B* **2004**, *108*, 1255–1266.

(39) Wang, J.; Kalinichev, A. G.; Kirkpatrick, R. J. Effects of substrate structure and composition on the structure, dynamics, and energetics of water at mineral surfaces: A molecular dynamics modeling study. *Geochim. Cosmochim. Acta* **2006**, *70*, 562–582.

(40) Teleman, O.; Jönsson, B.; Engström, S. A molecular dynamics simulation of a water model with intramolecular degrees of freedom. *Mol. Phys.* **1987**, *60*, 193–203.

(41) Abascal, J. L. F.; Vega, C. A general purpose model for the condensed phases of water: TIP4P/2005. *The Journal of Chemical Physics* **2005**, *123*, 234505.

(42) Thompson, A. P.; Aktulga, H. M.; Berger, R.; Bolintineanu, D. S.; Brown, W. M.; Crozier, P. S.; in 't Veld, P. J.; Kohlmeyer, A.; Moore, S. G.; Nguyen, T. D. et al. LAMMPS - a flexible simulation tool for particle-based materials modeling at the atomic, meso, and continuum scales. *Comput. Phys. Commun.* **2022**, *271*, 108171.

(43) Liu, P.; Harder, E.; Berne, B. J. On the calculation of diffusion coefficients in confined fluids and interfaces with an application to the liquid-vapor interface of water. *J. Phys. Chem. B* **2004**, *108*, 6595–6602.

(44) Tesson, S.; Louisfrema, W.; Salanne, M.; Boutin, A.; Ferrage, E.; Rotenberg, B.; Marry, V. Classical Polarizable Force Field to Study Hydrated Charged Clays and Zeolites. *J. Phys. Chem. C* **2018**, *122*, 24690–24704.

(45) Yeh, I.-C.; Hummer, G. System-Size Dependence of Diffusion Coefficients and Viscosities from Molecular Dynamics Simulations with Periodic Boundary Conditions. *J. Phys. Chem. B* **2004**, *108*, 15873–15879.

(46) Simonnin, P.; Noetinger, B.; Nieto-Draghi, C.; Marry, V.; Rotenberg, B. Diffusion under Confinement: Hydrodynamic Finite-Size Effects in Simulation. *J. Chem. Theory Comput.* **2017**, *13*, 2881–2889.

(47) Tazi, S.; Rotenberg, B.; Salanne, M.; Sprik, M.; Sulpizi, M. Absolute acidity of clay edge sites from ab-initio simulations. *Geochim. Cosmochim. Acta* **2012**, *94*, 1–11.

(48) Holz, M.; Heil, S.; Sacco, A. Temperature-dependent self-diffusion coefficients of water and six selected molecular liquids for .... *Phys. Chem. Chem. Phys.* **2000**, 1–3.

(49) Volino, F.; Perrin, J.-C.; Lyonnard, S. Gaussian Model for Localized Translational Motion: Application to Incoherent Neutron Scattering. *J. Phys. Chem. B* **2006**, *110*, 11217–11223.

(50) Qvist, J.; Schober, H.; Halle, B. Structural dynamics of supercooled water from quasielastic neutron scattering and molecular simulations. *J. Chem. Phys.* **2011**, *134*, 144508.

(51) Laage, D.; Hynes, J. T. On the residence time for water in a solute hydration shell: Application to aqueous halide solutions. *J. Phys. Chem. B* **2008**, *112*, 7697–7701.

(52) Luzar, A.; Chandler, D. Hydrogen-bond kinetics in liquid water. *Nature* **1996**, *379*, 55–57.

(53) Piskulich, Z. A.; Mesele, O. O.; Thompson, W. H. Activation Energies and beyond. *J. Phys. Chem. A* **2019**, *123*, 7185–7194.

TOC Graphic

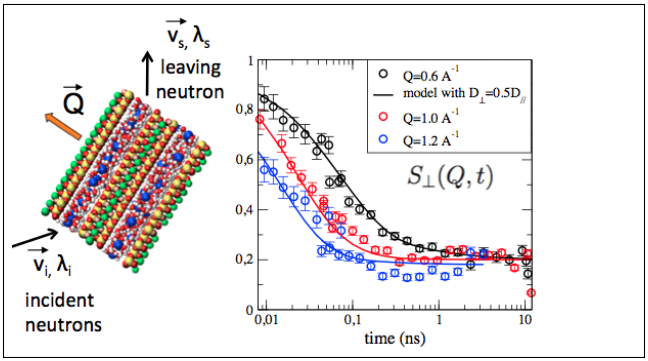

Some journals require a graphical entry for the Table of Contents. This should be laid out "print ready" so that the sizing of the text is correct.

Inside the `tocentry` environment, the font used is Helvetica 8 pt, as required by *Journal of the American Chemical Society*.

The surrounding frame is 9 cm by 3.5 cm, which is the maximum permitted for *Journal of the American Chemical Society* graphical table of content entries. The box will not resize if the content is too big: instead it will overflow the edge of the box.

This box and the associated title will always be printed on a separate page at the end of the document.